

<https://helda.helsinki.fi>

Overview of the JET ITER-like wall divertor

Widdowson, A.

2017

Widdowson , A , Alves , E , Baron-Wiechec , A , Barradas , N P , Catarino , N , Coad , J P , Corregidor , V , Garcia-Carrasco , A , Heinola , K , Koivuranta , S , Krat , S , Lahtinen , A , Likonen , J , Mayer , M , Petersson , P , Rubel , M , Van Boxel , S & JET Contributors 2017 , ' Overview of the JET ITER-like wall divertor ' , Nuclear Materials and Energy , vol. 12 , pp. 499-505 . <https://doi.org/10.1016/j.nme.2016.12.008>

<http://hdl.handle.net/10138/228801>

<https://doi.org/10.1016/j.nme.2016.12.008>

cc_by_nc_nd

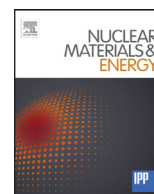
publishedVersion

Downloaded from Helda, University of Helsinki institutional repository.

This is an electronic reprint of the original article.

This reprint may differ from the original in pagination and typographic detail.

Please cite the original version.



Overview of the JET ITER-like wall divertor



A. Widdowson^{a,*}, E. Alves^b, A. Baron-Wiechec^a, N.P. Barradas^c, N. Catarino^b, J.P. Coad^a, V. Corregidor^b, A. Garcia-Carrasco^h, K. Heinola^d, S. Koivuranta^e, S. Krat^{f,g}, A. Lahtinen^d, J. Likonen^e, M. Mayer^f, P. Petersson^h, M. Rubel^h, S. Van Boxel^a, JET Contributors^{1,2}

^a CCFE, Culham Science Centre, Abingdon, OX14 3DB, UK

^b IPFN Instituto Superior Técnico, Universidade de Lisboa, 1049-001 Lisboa, Portugal

^c C²TN, Instituto Superior Técnico, Universidade de Lisboa, 2695-066 Lisboa, Portugal

^d University of Helsinki, P.O. Box 64, 00560 Helsinki, Finland

^e VTT Technical Research Centre of Finland, P.O. Box 1000, FIN-02044 VTT, Finland

^f Max-Planck Institut für Plasmaphysik, 85748 Garching, Germany

^g National Research Nuclear University MEPhI, 115409 Moscow, Russia

^h Royal Institute of Technology, SE-10044 Stockholm, Sweden

ARTICLE INFO

Article history:

Received 14 July 2016

Revised 30 November 2016

Accepted 7 December 2016

Available online 16 February 2017

Keywords:

Jet

Erosion

Deposition

Fuel retention

Dust

Tungsten coating

ABSTRACT

The work presented draws on new analysis of components removed following the second JET ITER-like wall campaign 2013–14 concentrating on the upper inner divertor, inner and outer divertor corners, life-time issues relating to tungsten coatings on JET carbon fibre composite divertor tiles and dust/particulate generation. The results show that the upper inner divertor remains the region of highest deposition in the JET-ILW. Variations in plasma configurations between the first and second campaign have altered material migration to the corners of the inner and outer divertor. Net deposition is shown to be beneficial in the sense that it reduces W coating erosion, covers small areas of exposed carbon surfaces and even encapsulates particles.

© 2017 Elsevier Ltd.

This is an open access article under the CC BY-NC-ND license.

(<http://creativecommons.org/licenses/by-nc-nd/4.0/>)

1. Introduction

Following each JET ITER-like wall (JET-ILW) campaign a set of plasma facing components (PFC) have been removed for surface analysis. Results from the analysis of these components provide direct measurement of material erosion, deposition, fuel retention, composition and morphology. In conjunction with campaign statistics, such as the distribution of strike points in the divertor or plasma operation times, an insight into the key plasma parameters driving erosion, deposition, material migration and fuel retention may be obtained. The results may be considered individually giving local erosion/deposition phenomena or collectively enabling global material migration and fuel retention patterns for JET-ILW to be mapped.

Two experimental campaigns have now been completed with the JET-ILW; 2011–2012 (ILW-1) and 2013–2014 (ILW-2). A comprehensive assessment following ILW-1 shows that global fuel retention was ~0.2% of injected fuel (deuterium, D) which is at least an order of magnitude lower than the JET carbon wall (JET-C). Of this ~65% of the retained fuel is found in the divertor and remote divertor corners, with the remaining inventory located in the main chamber [1]. The results presented here for ILW-2 focus on local phenomena and comparison with ILW-1. Extrapolations to global long term fuel retention and material migration will be the subject of future publications.

2. Experimental details

The fuel retention, material erosion/deposition, composition and morphology results for samples removed from JET are drawn from a range of surface analysis techniques including; ion beam analysis techniques (IBA) [2,3,4], secondary ion mass spectrometry (SIMS) [1,5], thermal desorption spectrometry (TDS) [6], surface profilometry [7], electron microscopy with elemental analysis capability using energy dispersive spectroscopy (EDS) [8] and optical microscopy. References give details of the techniques and examples

* Corresponding author.

E-mail address: anna.widdowson@ukaea.uk (A. Widdowson).

¹ See the Appendix of F. Romanelli et al., Proceedings of the 25th IAEA Fusion Energy Conference 2014, Saint Petersburg, Russia

² EUROfusion Consortium, JET, Culham Science Centre, Abingdon, OX14 3DB, UK

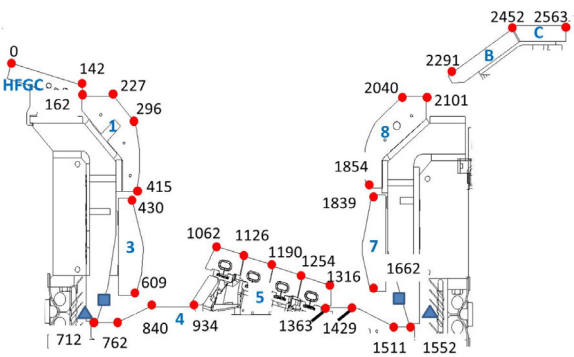


Fig. 1. Cross section of JET-ILW divertor showing tile numbering and the s -coordinate; distance around the divertor surface in millimetres. Tile 1 apron is in the region $s = 162$ – 227 mm. Tile 5 is also referred to as the bulk tungsten tile. ▲ shows the location of louvre clips. ■ shows the location of mirrors.

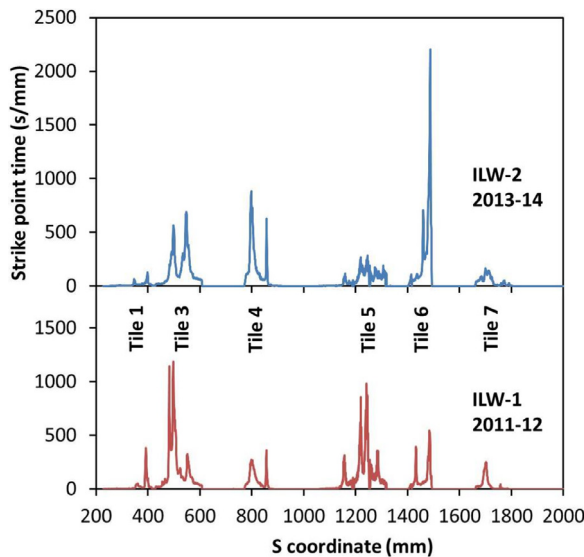


Fig. 2. Strike point distribution for ILW-1 (2011–12) and ILW-2 (2013–14).

of analysis of JET components using these techniques. Whilst some whole JET tiles and components are analysed it is usually necessary to reduce the overall size of samples for analysis e.g., cut cores or prepare polished cross sections from tiles as described in [9] and references therein.

The analysed data are presented using JET tile numbering terminology and s -coordinate system (distance along the divertor surface in millimetres) as shown in Fig. 1. It should be noted that the s -coordinate system has been updated for JET-ILW compared with JET-C to account for the increase in divertor surface length in the poloidal direction arising from the installation of the bulk tungsten (W) Tile 5 assemblies. The comparison of results from ILW-1 and ILW-2 are discussed in the context of strike point distribution and plasma operation times. The distribution of the inner strike points (ISP) $s < 934$ mm and outer strike points (OSP) $s > 1062$ mm are shown in Fig. 2. There are variations with the ISP being predominantly on the surface of the vertical inner divertor Tile 3 for ILW-1 and the inner divertor corner Tile 4 for ILW-2 and the OSP being predominantly on bulk W Tile 5 for ILW-1 and outer divertor corner Tile 6 for ILW-2. Total plasma time per operating period is calculated by taking into account both commissioning and campaign JET pulses with plasma current > 0.25 MA; no weighting is given to additional plasma heating. Divertor plasma time is defined when the strike points are below the vessel height of $z = -1.4$ m (from the vessel mid-plane where $z = 0$ m). Limiter plasmas are

taken as the remaining time from the total. The overall plasma times for ILW-1 and ILW-2 are 6 / 5.2 h limiter plasma and 13 / 14.2 h divertor plasma respectively. ILW-1 ended with 125 identical D plasma pulses with the ISP on Tile 3, the OSP on the bulk W Tile 5 and ~ 12 MW neutral beam heating per pulse. Whereas ILW-2 ended with a hydrogen (H) campaign with a varied plasma configuration programme. Approximately 300 JET pulses were performed in H, $\sim 10\%$ of the total number of JET pulses throughout the campaign, or 0.6 h. Early during the H campaign neutral beam heating was available however throughout most of this period there were generally lower power pulses with ICRH heating (< 6 MW) and Ohmic plasmas. During the H campaign experiments nitrogen (N) was also injected. The results for N are not discussed in this contribution but are found elsewhere [10].

JET-ILW divertor tiles consist of $\sim 25 \mu\text{m}$ W coatings with a $3 \mu\text{m}$ Molybdenum (Mo) interlayer layer on carbon fibre composite substrates (W-CFC). In addition two coating variations known as *marker coatings* were installed for a subset of divertor tiles during ILW-1 and ILW-2; a *W marker coating* with nominal thickness CFC/ $3 \mu\text{m}$ Mo/ $12 \mu\text{m}$ W/ $4 \mu\text{m}$ Mo/ $4 \mu\text{m}$ W and *Mo marker coating* with nominal thickness CFC/ $3 \mu\text{m}$ Mo/ $12 \mu\text{m}$ W/ $4 \mu\text{m}$ Mo. The aim of having a few tiles with a final Mo coating was to enable the local transport of W within the divertor to be assessed.

After ILW-2 and before removing any PFCs the divertor tile surfaces were vacuumed using a vacuum cleaner with a cyclone to collect JET dust and particulates into pots attached below the cyclone. The methodology for the vacuum dust collection after ILW-2 was identical to that of ILW-1 for which details of the vacuum equipment, vacuuming scheme and corrections applied to the mass of dust collected can be found in [11]. In brief, the vacuuming was completed in two stages. A sample for the outer divertor surface (Tiles 5, 6, 7, 8, B, C) was collected into one cyclone pot and a sample for the inner divertor surface (Tiles HFGC, 1, 3, 4) was collected into a second cyclone pot. The divertor tiles allocated for *post mortem* analysis were not vacuumed; therefore only 11/12th of the divertor surface was vacuumed. The cyclone pots were weighed before and after dust collection to determine the amount of dust collected. In addition to vacuuming, dust samples were collected directly from non-vacuumed divertor tile surfaces using adhesive carbon pads on microscopy sample stubs. These samples were analysed using electron microscopy.

3. Results

The following sub-sections summarise erosion and deposition analysis from different regions of the JET divertor surface.

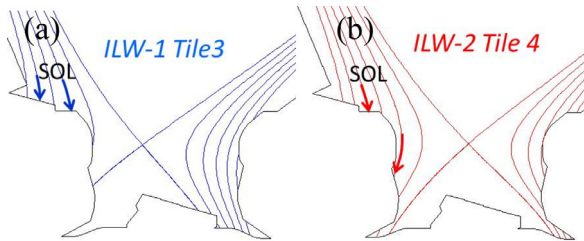
3.1. Upper inner divertor

The upper inner surface of the JET divertor ($s = 0$ – 296 mm, see Fig. 1) remains an area of high deposition for ILW-2 as was observed for ILW-1. Surface profilometry, microscopy of cross sections cut from tiles, IBA and depth profiling using SIMS were used to determine the thickness of deposit at the top of the inner divertor. The thicknesses are summarised for ILW-2 and ILW-1 in Table 1. The predominant ISP location, which has moved from Tile 3 in ILW-1 to Tile 4 in ILW-2 as seen in Fig. 2, plays a role in the distribution of the deposition. The downward movement of the ISP position extends the surface area over which ion fluxes transported in the SOL are deposited; HFGC/Tile 1 apron ($s = 0$ – 227 mm) for ILW-1 as illustrated in Fig. 3(a) and HFGC/Tile 1 apron/upper vertical surface ($s = 142$ – 296 mm) down to the bottom of Tile 1 ($s = 296$ – 415 mm) for ILW-2 as illustrated in Fig. 3(b). The results presented in Table 1 show that deposits $\sim 10 \mu\text{m}$ thick extend further down Tile 1, to $s = 296$ mm, after ILW-2 compared with ILW-1 where similar thickness deposits end at $s = 227$ mm. In addition, from IBA re-

Table 1

Summary of deposition at upper inner divertor corner ILW-1 and ILW-2. *ILW-1 values are taken from [11] and [12].

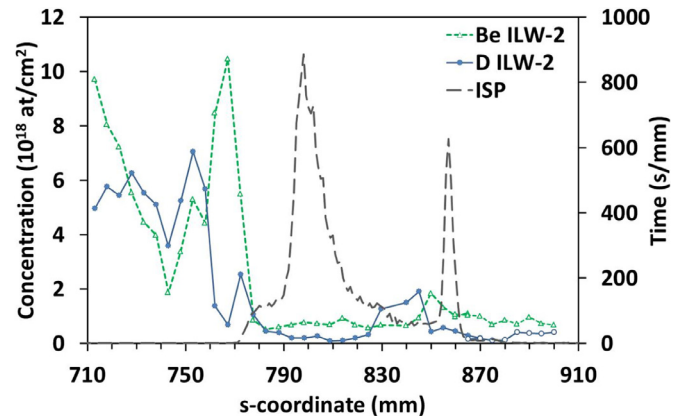
Campaign exposure	Tile description	s-coordinate (mm)	Analysis technique	Deposit thickness (μm)
ILW-1*	Tile 1 apron	162–227	IBA & Microscopy	≥ 10 –15
ILW-1*	HFGC	42–142	IBA	3–8
ILW-1&2	HFGC	42–142	Profilometry	30–50
		135	SIMS	40
ILW-2	Tile 1 apron and upper vertical surface	216	SIMS	~ 10
		162–296	IBA	10

**Fig. 3.** Field lines for predominant inner strike point position in (a) ILW-1 and (b) ILW-2.

sults deposits of the order 1–2 μm extend to $s = 415$ mm for ILW-2 whereas deposits are an order of magnitude less in the same region for ILW-1. The cumulative thickness of deposit on the HFGC tile following ILW-1&2 is significantly higher than the deposit after ILW-1, indicating deposition of 20–40 μm during ILW-2. This is significantly higher than the $\sim 10 \mu\text{m}$ deposit on the top of Tile 1 after ILW-2 suggesting that the area of greatest deposition during ILW-2 was on the HFGC tile ($s = 0$ –142 mm) as opposed to the top of Tile 1 ($s = 162$ –296 mm) and that ion fluxes remain high deep in the SOL where the HFGC tile was predominantly located during ILW-2.

SIMS and IBA measurements in this region show that deposits are beryllium (Be) dominated [2]. At the top vertical surface of Tile 1 Be deposition is $\sim 4.5 \times 10^{19}$ at./cm² after ILW-2. Assuming that deposition occurs during divertor plasma configurations the Be deposition rate is $\sim 0.9 \times 10^{15}$ at./cm² s. Modelling with WALL-Dyn [13] shows that the top of the inner divertor is an area of net deposition with a deposition rate of 0.4 – 2.8×10^{16} at./cm² s on the Tile 1 apron ($s = 162$ –227 mm) depending on modelling assumptions. As discussed in [13], the higher deposition rates from modelling may be due to the relatively lower steady state divertor time used in modelling compared with the total divertor time used to determine experimental deposition rates.

IBA and SIMS analysis show evidence of depletion of D within the first few microns of the surface of the HFGC and Tile 1 following ILW-2. This is likely to be due to a combination of co-deposition with H injected into the vessel at the end of ILW-2 and isotopic exchange at the surface of the tile. For ILW-1 IBA results show D concentrations were proportional to the Be concentration in that D concentration was 3 – 10×10^{18} at./cm² in the deposits on the top of Tile 1 ($s = 162$ –296 mm) which decreased to $< 1 \times 10^{18}$ at./cm² in the region of little or no deposition at the bottom of Tile 1 ($s = 296$ –415 mm). Following ILW-2 the concentration of D remained relatively constant across Tile 1, with D concentrations of 1 – 3×10^{18} at./cm² in deposits ($s = 162$ –296 mm) and 1 – 2×10^{18} at./cm² in regions of little or no deposit ($s = 296$ –415 mm). Similar effects are observed with SIMS where D concentration is shown to be depleted to a depth of $\sim 2 \mu\text{m}$, whilst H concentration peaks at the surface. The peak in H concentration at the surface is much more pronounced in the ILW-2 samples following H operation than for ILW-1 samples measured using SIMS and elastic recoil detection analysis (ERDA). This indicates that H is deposited to greater depths in the ILW-2 samples which cannot solely be due to

**Fig. 4.** Ion beam analysis results for Tile 4 inner divertor corner.

exposure in atmosphere once removed from the vessel. The depletion of D from the surface of tiles will have the greatest effect on fuel retention calculations where thin deposits occur - in regions of thick deposits buried layers will still trap fuel.

3.2. Inner divertor corner

The ISP was on the inner divertor corner Tile 4 at $s = 800$ mm for ~ 3 times longer during ILW-2 than for ILW-1, see Fig. 2. This has altered the material migration pattern between the two campaigns with more material migrating to Tile 4. A darker band of deposit was observed at the bottom of the sloping surface on Tile 4 ($s = 762$ mm) after ILW-2 than after ILW-1. This deposition band extends toroidally and is ~ 10 mm wide in the poloidal direction. Fig. 4 shows Be and D deposition on Tile 4 in the poloidal direction and the ISP distribution for ILW-2. Analysis using IBA shows that there is up to 10 times more Be deposition in this band compared with the same location after ILW-1 (1×10^{18} at./cm²). The band is located ~ 30 mm beyond the ISP location. The Be and D deposition also extends to the plasma shadowed surface of Tile 4 ($s = 712$ –762 mm); the concentrations are up to 10×10^{18} Be at./cm² and 7×10^{18} D at./cm².

Moving further into the remote inner corner, Fig. 5 shows the deposition of Be, D and C on a mirror surface and louvre clip. The louvre clip is mounted inboard of the innermost corner of Tile 4 whilst the mirror is mounted higher and closer to the plasma, just below Tile 3, the approximate locations are indicated in Fig. 1. The clip is mounted on to an actively cooled louvre fin and the mirror is held in a metallic holder which in turn is mounted onto a carbon rib structure with no cooling. The IBA results presented for the mirror [10] and clip are from surfaces facing toward the centre line of the machine; the clip surface is ~ 50 mm radially inward (i.e. more recessed) than the mirror surface. The discussion below makes the following comparisons of the IBA data presented in Fig. 5: (i) a comparison of ILW-1 and ILW-2 deposition; (ii) a comparison of the deposition on the clip and mirror for each ILW campaign and (iii) a comparison with deposition on Tile 4.

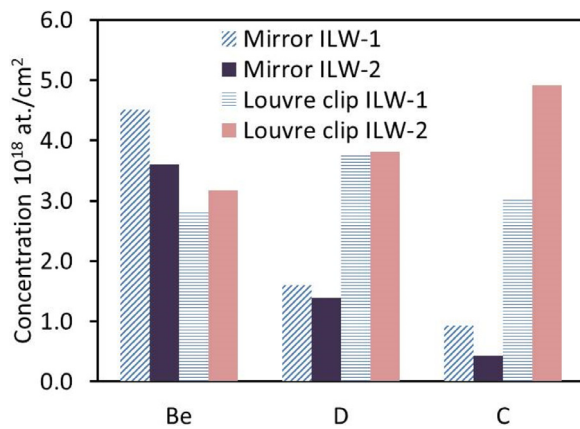


Fig. 5. Deposition at mirror and louvre clip surfaces located in the remote inner divertor corner.

Comparing between ILW-1 and ILW-2 campaigns; for the mirror the Be and D have decreased by $<20\%$ and for the clip Be and D have increased by $\sim 10\%$. There is a larger change in C concentrations, but the overall trend remains a decrease on the mirror and an increase on the clip as for Be and D. It is striking that the increase in the time of the ISP on Tile 4 for ILW-2 compared with ILW-1 which is expected to result in an increase in flux to this region has not had a significant impact on line-of-sight deposition at the remote inner corner - there is a relatively small variation in Be, D and C deposition between ILW-1 and ILW-2 for the mirror and clip. In contrast the local/prompt deposition of Be on Tile 4 has increased significantly along with deposition on the remote horizontal tile surface ($s = 712 - 726$ mm). Comparing the data for the mirror with that of the clip for each ILW campaign the D and C concentration are lower for the mirror than the clip whereas the Be concentration is slightly higher. The lower D and C may be due to higher surface temperatures of the mirror surface which is closer to the plasma, whereas the clip is mounted on cooled louvre structures resulting in higher deposition of D and C. However this does not fully explain the Be deposition distribution. Comparing the mirror and clip with the end of Tile 4 for ILW-2; the Be deposition on the clip and mirror is lower than observed on the end of Tile 4 ($s = 712 - 740$ mm, see Fig. 4).

The results elucidate two transport mechanisms at the extreme of the ISP location; one of local re-deposition of ionised particles either sputtered or reflected at the SP forming a band of deposition ~ 30 mm inboard of the ISP location and another of line-of-sight transport of neutrals to the remote inner corner giving rise to deposition on the shadowed surface of Tile 4, the mirror and clip. For line-of-sight transport of neutrals the geometry from the ISP location with respect to the remote deposition surfaces will influence the amount of material deposited. The line-of-sight transport of neutrals to the remote inner corner when the ISP is on Tile 4 was previously demonstrated for ILW-1 using a rotating deposition collector [14,15]. The surface temperature of the remote deposition surfaces will also affect deposition; variations in surface temperature may occur due to proximity of the plasma and thermal properties related to the mounting location. In addition to these factors a full explanation of the material migration and fuel retention requires further investigation of the fluxes reaching the inner corner during divertor plasmas.

3.3. Outer divertor corner

During ILW-2 the OSP was predominantly on the outer divertor corner Tile 6 at $s = 1487$ mm for ~ 3 times longer than during ILW-1 when the OSP was predominantly on the bulk W

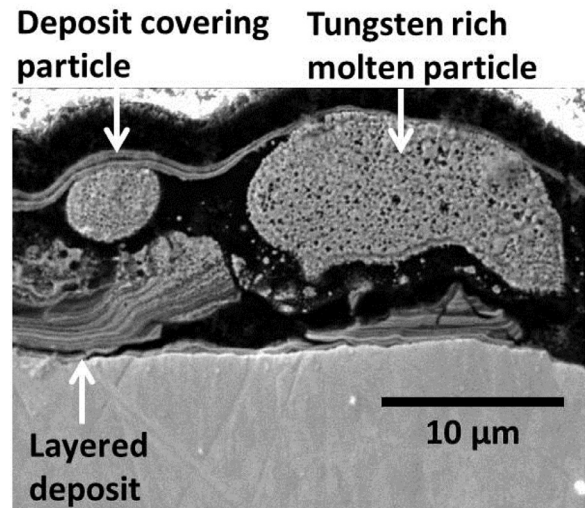


Fig. 6. SEM image showing layered deposit and metallic droplet encapsulated with over laying deposit.

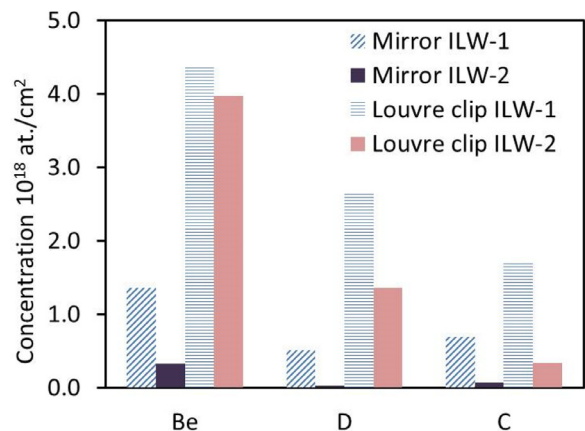


Fig. 7. Deposition at mirror and louvre clip surfaces located in the remote outer divertor corner.

Tile 5. As for the inner divertor Tile 4 there is a Be-rich band of deposition (32.6×10^{18} at./cm²) outboard of the OSP location at $s = 1511$ mm extending toroidally across the tile and ~ 10 mm wide in the poloidal direction which was not as obvious after ILW-1. The thickness of the band of deposit is ~ 6 times greater than for ILW-1. A cross section taken from this region shows that the deposit consists of a layered structure with a total thickness of 2–3 μm see Fig. 6. The D concentration (1.5×10^{18} at./cm²) is also peaked in this deposition band whereas for ILW-1 the D distribution extended along the outer sloping plasma accessible surface of Tile 6 ($s = 1429 - 1511$ mm) at a concentration of $0.8 - 1.6 \times 10^{18}$ at./cm². The decrease in D concentration on the sloping surface to $\sim 0.1 \times 10^{18}$ at./cm² in ILW-2 is likely due to difference in surface temperatures arising from the OSP location on Tile 6 and also co-deposition and isotopic exchange in H plasmas as discussed in 3.1.

A similar set up of a clip and mirror exists in the remote outer divertor corner as for the inner divertor corner. The results from IBA are shown in Fig. 7 and the discussion is developed in a similar way to Section 3.2. Comparing ILW-2 and ILW-1 the clip shows a decrease in D and C deposition in the outer divertor whereas Be remains similar. For the mirror deposition is significantly lower for ILW-2 than ILW-1. Comparing the data for the mirror with that of the clip for each ILW campaign the deposition on the mirror is

generally lower than on the clip. This is likely to be due to the difference in proximity of the mirror surface and clip surface to the OSP which alters surface temperatures and geometry. In the outer divertor corner the mirror is located just below Tile 7. When the OSP is deep into the outer corner, the line-of-sight angle subtended from the OSP to the front of the mirror is shallow. This makes a significant difference in the geometrical effects compared with ILW-1 when the OSP was on Tile 5. Heating in this region will also be higher for ILW-2 due to the OSP being close to the mirrors which will act to reduce deposition. The clip is located close to the outermost corner of Tile 6 with a more direct line-of-sight from the OSP than the mirror. In addition the clip is radially further outboard into the corner compared to the mirror by ~ 50 mm and is mounted on an actively cooled louvre fin. Whilst a detailed geometrical and temperature study has not been completed, these conditions are conducive to higher deposition on the clip than the mirror. As seen for the inner divertor corner, the presence of a band of deposition just beyond the OSP shows prompt deposition of ionised species whilst deposition onto the mirror and clip shows line-of-sight transport of neutrals.

3.4. Tungsten coating lifetime

Two aspects of tungsten coating are crucial for coating lifetime assessment; (i) erosion of the coatings exposed to plasma and (ii) coating integrity. W/Mo marker coatings on divertor tiles have been analysed to assess W coating lifetime issues. IBA of the inner divertor Tile 4 with Mo marker surface exposed during ILW-2 shows that $\sim 1.8 \mu\text{m}$ (12×10^{18} at./ cm^2) of Mo was eroded from the surface of the tile at the location of the ISP [2]. At the same time there is W deposition at the ISP location and also a thinner band of W deposition inboard of the strike point. This is indicative of a net ion flux of W coming to the surface of the inner divertor corner along with Be and D. As discussed in Section 3.2, the deposited D and Be undergoes sputtering and is either locally re-deposited or migrates to the inner corner. For W the sputtering yield is much lower than for Be therefore the deposited W remains mainly at the ISP location. Consequently only a relatively small fraction is re-eroded and subsequently redeposited either locally or remotely. Indeed small amounts of W ($< 50 \times 10^{15}$ at./ cm^2) are seen at the inner corner.

Cross sections were prepared for the upper part of Tile 3 with W marker coating at the inner divertor ($s = 435\text{--}490$ mm) exposed during ILW-1 & 2 and analysed using optical microscopy. In the region $s = 435\text{--}453$ mm at the top of Tile 3 there are areas where the $4 \mu\text{m}$ W coating is completely eroded and partial erosion of the Mo layer below. In addition deposits up to $10 \mu\text{m}$ thick are observed on the top surface. In the region $s = 453\text{--}471$ mm, lower down Tile 3, there is partial erosion of the W layer in some areas with no erosion of the Mo layer beneath. Again a deposit has formed at the surface. In the region $s = 471\text{--}490$ mm there is no evidence of erosion of the W coating and a small amount of deposit $\sim 1\text{--}2 \mu\text{m}$ observed at the surface. IBA and glow discharge optical emission spectroscopy (GDOES) [16] for a Tile 3 exposed during ILW-1 showed that most erosion (Mo in the case of this particular tile) occurred at the top of Tile 3 ($s = 435\text{--}490$ mm), with the maximum at $s \sim 445$ mm [3] with a deposit overlaying the surface.

Both Tile 4 and Tile 3 results show erosion of coatings with deposits overlaying the surface. The likeliest explanation for the results is that at the start of a campaign when the divertor tiles are new erosion occurs; however overall the inner divertor surface is a region of net deposition and Be rich deposits subsequently cover coatings. Indeed modelling indicates the suppression of W erosion under conditions of Be irradiation due to the formation of Be deposits and W-Be mixed layers [17,18]. For Tile 4 there is a clear correlation with the ISP location giving rise to erosion and subse-

quent deposition. However for Tile 3 the ISP did not dwell for a significant length of time at the location of highest coating erosion ($s = 435\text{--}453$ mm). The ISP was mainly located at $s = 498$ mm and 548 mm during ILW-2 which would result in the top of Tile 3 being in the SOL and remaining a net deposition zone. Therefore the period during which the W erosion occurred early in the campaign would require further analysis of the time evolution of the ISP with JET pulse number as well as an understanding of the particle fluxes reaching the inner divertor and ELMs affecting effective W sputtering yields [19].

The erosion rate of the W coatings does not exceed more than $\sim 2 \mu\text{m}$ per campaign. A precise erosion rate is somewhat uncertain due to the difficulties in ascertaining when during the campaign and for how long erosion occurred. If the erosion is considered to take place at the ISP location, then by normalising to the divertor plasma time a lower erosion rate $\sim 0.23 \times 10^{15}$ at./ cm^2s is determined for the Mo marker coated Tile 4 (ILW-2). However if erosion only takes place for a limited period before a deposit builds up on the surface then a higher initial erosion rate is likely. Erosion from bulk W PFCs has not been directly measured and is expected to be lower. However redeposited W will erode at a faster rate and migrate in small quantities via a cycle of re-erosion/re-deposition to remote areas.

Delamination of tungsten coatings on a few CFC based tiles was observed after ILW-2. This is associated with tiles which did not fully undergo the prescribed heat treatment at the time of production. The issues predominantly occur on outer divertor corner tiles 6 in a region of significant heat load which has resulted in a pattern of film cracking and delamination along CFC fibre planes perpendicular to the tile surface and in a poloidal orientation along the tile. By eye the delaminated areas appear to reveal the CFC tile below, raising a cause for concern that this could be a source of C in the plasma. However IBA data, including micro-beam Proton Induced X-ray Emission (PIXE) mapping, show that Be and other heavy elements (W and Mo) are present on the delaminated surfaces. In addition SEM micrographs of cross sections show no evidence of erosion from the CFC surface and that thin deposits have formed in delaminated regions. There is a known mechanism for failure of the coatings by carbide formation if surface temperatures exceed 1350°C for > 2 h [20], however JET operating instructions are used to prevent this degree of surface heating and therefore this mechanism has not been identified in the samples analysed thus far. Crucially the results of this analysis shows that despite the delamination of the W coating, the exposed surfaces are covered either by residual coating or deposits and do not therefore contribute to C in the machine. This is also supported by the significant decrease in C migrating to the remote outer divertor corner in ILW-2 compared with ILW-1 as shown in Fig. 7.

3.5. JET dust and particulates

The mass of dust collected by vacuuming was 0.39 g and 0.98 g at the inner and outer surfaces respectively, giving a total mass of dust present on the inner and outer divertor surfaces after corrections as described in [11] as 0.45 g and 1.37 g respectively. These values are similar in magnitude to the dust collected from ILW-1; 0.7 g and 0.3 g [11] or 0.86 g and 0.38 g after corrections are applied. The largest error in the dust collection exercise is associated with the consistency of the vacuuming method using remote handling equipment, therefore no detailed comparison is made between the amounts of dust collected at the inner and outer divertor for ILW-1 and ILW-2.

One potential source of particles in the divertor is from the disintegration of thick deposits, as seen in JET-C. The fact that the dust masses remain low indicates that deposits have not yet started to spall. The thickest deposits observed so far are $\sim 40 \mu\text{m}$

at the upper inner divertor as described in Section 3.1. Photographs of the Tile 1 *apron* show that a rough deposit has formed. The deposit, whilst rough, is well adhered to the surface – in that it was not removed when taking dust samples from the surface with adhesive pads – and does not show signs of disintegration after two campaigns (38.4 h total plasma time and 27.2 divertor plasmas) and exposure to atmosphere following vessel interventions. However, as deposits accumulate in this region in subsequent campaigns it is likely that the deposit will eventually start to disintegrate. One area where delamination of deposits is observed is on the metallic surface of an inner mirror exposed during ILW-2 and the mounting bracket exposed during ILW-1&2, located in the remote inner divertor corner. These are Be-rich deposits with oxygen, N and C which consist of several 100 – 150 nm delaminating layers [10]. These deposits are not characteristic of deposits forming on remote PFCs as the mirror is a polished surface therefore the adhesion of the deposit is expected to be lower than for comparatively rougher surfaces of PFCs.

The survey of dust and particulates collected on to adhesive pads shows a varied selection of species dependent on collection location. At the upper inner divertor flakes and debris in the size range 30 – 100 μm were observed. Compositional analysis shows particles originating from the Be coating covering recessed inner wall cladding, Be dominated particles probably from molten zones of Be main chamber tiles, and W-Ni particles with low Z element inclusions. At the outer divertor corner particles include flakes of Be deposits and fragments of W coatings delaminated from divertor tiles. One aspect that has been observed from SEM micrographs is that of molten particles encapsulated by deposit forming over them as shown in Fig. 6. The extent of this particle capture mechanism is not accessed but it may have some bearing on reducing dust mobility in net deposition areas.

4. Discussion and conclusion

Be erosion in the main chamber by charge exchange neutrals at the first wall during diverted plasma configurations followed by transport in the SOL to the divertor is still the main material migration mechanism in JET. However *post-mortem* analysis of individual tiles from the JET divertor enables a detailed picture of deposition and subsequent material migration within the divertor to be established. The results show that deposition and erosion is strongly dependent of plasma configuration, i.e., location of inner and outer strike points during operations. The results show that the upper inner divertor remains the region of highest deposition and the dominant region for fuel retention with co-deposits up to 40 μm after exposure for two campaigns. This surface is in the SOL, does not undergo strong plasma interaction and generally does not exceed surface temperatures of 300 °C, therefore material deposited in this region is not eroded and fuel is not desorbed.

Noticeable differences are observed at the inner and outer divertor corners when comparing deposition for ILW-1 and ILW-2. On the inner and outer corner tiles (Tiles 4 and 6) a band of Be-rich deposit has formed inboard/outboard of the inner/outer SP locations respectively in ILW-2. This deposition occurs as a result of prompt deposition of ionised species just beyond the plasma accessible region and is much thinner than deposits at the upper inner divertor. In more remote parts of the divertor, line-of-sight transport and deposition of neutrals show that Be and small amounts of W, along with D and C, have a migration path to remote surfaces and that deposition rates show a strong dependence on geometry and surface temperature.

The depletion of D at the surface of deposits observed on Tile 1 and Tile 6 is likely due to finishing the ILW-2 campaign in hydrogen. These results show that a combination of co-deposition with H and isotope exchange reduces fuel content in the first few mi-

crons of deposits but that thick deposits on plasma accessible surfaces and remote regions will remain a source of fuel retention; therefore alternative fuel removal methods will be needed in ITER to manage fuel inventory.

A new aspect of JET-ILW tile analysis is the evaluation of W coatings on CFC tiles. First results indicate that erosion of coatings is < 2 μm per campaign. *Post mortem* analysis suggests that in areas of net deposition erosion only occurs for a relatively short period and ceases altogether once a deposited layer is formed. The formation of Be deposits in the outer divertor corner is also beneficial in mitigating the erosion of C where coating delamination has occurred.

The deposit at the top of the inner divertor is now up to 40 μm thick after 27.2 h of divertor plasmas and is still well adhered to the tile even following exposure in air. As a consequence dust production from disintegrating deposits is still low, with < 2 g of dust being present on divertor tile surfaces. Although this is positive news for the ITER divertor, the integrity of deposits in the JET divertor will be closely monitored in following interventions. A survey of particles collected show a range of sources; W/Mo divertor tile coatings, molten Be, Be-rich deposits. Analysis of a tile cross section shows evidence of dust particles immobilised due to deposits forming over them. This is a potential benefit for ITER in partially reducing mobilisable dust quantities and reactive surface area of dust particles on plasma facing surfaces.

Overall the analysis shows that co-deposition of D continues to be the main fuel retention mechanism and the accumulation of deposit at the top of the inner divertor accounts for a majority of material migrating from the main chamber to the divertor. Changes in the plasma configurations have not had a major impact on these dominating phenomena.

These results show how *post mortem* analyses of tiles and passive diagnostics are used for the direct measurement of material migration, erosion/deposition and fuel retention on plasma facing and remote surfaces. The results demonstrate that small probes located in the ITER divertor would enable local and global phenomena to be periodically analysed to provide direct measurements for benchmarking with real time systems.

Acknowledgements

This work has been carried out within the framework of the EUROfusion Consortium and has received funding from the Euratom research and training programme 2014–2018 under grant agreement No 633053. The views and opinions expressed herein do not necessarily reflect those of the European Commission. This work was also part-funded by the RCUK Energy Programme under grant EP/I501045.

References

- [1] K. Heinola, A. Widdowson, J. Likonen, E. Alves, A. Baron-Wiechec, N. Barradas, S. Brezinsek, N. Catarino, P. Coad, S. Koivuranta, S. Krat, G.F. Matthews, M. Mayer, P. Petersson, JET-Contributors, Phys. Scr. T167 (2016) 014075. <http://dx.doi.org/10.1088/0031-8949/T167/1/014075>.
- [2] N. Catarino, N.P. Barradas, V. Corregidor, A. Widdowson, A. Baron-Wiechec, J.P. Coad, K. Heinola, M. Rubel, E. Alves, JET Contributors, in press Nuclear Materials and Energy. 2016. <http://dx.doi.org/10.1016/j.nme.2016.10.027>.
- [3] M. Mayer, S. Krat, W. Van Renterghem, A. Baron-Wiechec, S. Brezinsek, I. Bykov, P. Coad, Yu. Gasparyan, K. Heinola, J. Likonen, A. Pisarev, C. Ruset, G. de Saint-Aubin, A. Widdowson, JET Contributors, Phys. Scr. T167 (2016) 014051.
- [4] P. Petersson, M. Rubel, H.G. Esser, J. Likonen, S. Koivuranta, A. Widdowson, JET-EFDA Contributors, J. Nucl. Mater. 463 (2015) 814. <http://dx.doi.org/10.1016/j.jnucmat.2014.12.077>.
- [5] S. Koivuranta, J. Likonen, A. Hakola, J.P. Coad, A. Widdowson, D.E. Hole, M. Rubel, JET-EFDA Contributors, Phys. Scr. T 159 (2014) 014052. <http://dx.doi.org/10.1088/0031-8949/2014/T159/014052>.

- [6] J. Likonen, K. Heinola, A. De Backer, S. Koivuranta, A. Hakola, C.F. Ayres, A. Baron-Wiechec, P. Coad, G.F. Matthews, A. Widdowson, JET Contributors, *Phys. Scr.* T167 (2016) 014074. <http://dx.doi.org/10.1088/0031-8949/T167/1/014074>.
- [7] A. Widdowson, C.F. Ayres, S. Booth, J.P. Coad, A. Hakola, K. Heinola, D. Ivanova, S. Koivuranta, J. Likonen, M. Mayer, M. Stamp, JET-EFDA Contributors, *J. Nucl. Mater.* 438 (2013) S827.
- [8] A. Baron-Wiechec, E. Fortuna, J. Grzonka, M. Rubel, A. Widdowson, C. Ayres, J.P. Coad, K. Heinola, G.F. Matthews, JET Contributors, *Nucl. Fus.* 55 (2015) 113033. <http://stacks.iop.org/0029-5515/55/113033>.
- [9] A. Widdowson, A. Baron-Wiechec, J.P. Coad, K. Heinola, J. Likonen, C. Lungu, G.F. Matthews, M. Rubel, JET Contributors, *Phys. Scr.* T167 (2016) 014057. <http://dx.doi.org/10.1088/0031-8949/T167/1/014057>.
- [10] A. Garcia-Carrasco et al., in press *Nuclear Materials and Energy* 2016 <http://dx.doi.org/10.1016/j.nme.2016.12.032>
- [11] A. Widdowson, E. Alves, C.F. Ayres, A. Baron-Wiechec, S. Brezinsek, N. Catarino, J.P. Coad, K. Heinola, J. Likonen, G.F. Matthews, M. Mayer, M. Rubel, JET-EFDA Contributors, *Phys. Scr.* T159 (2014) 014010. <http://dx.doi.org/10.1088/0031-8949/2014/T159/014010>.
- [12] A. Baron-Wiechec, A. Widdowson, E. Alves, C.F. Ayres, N.P. Barradas, S. Brezinsek, J.P. Coad, N. Catarino, K. Heinola, J. Likonen, G.F. Matthews, M. Mayer, P. Petersson, M. Rubel, W. van Renterghem, I. Uytendhouwen, JET-EFDA Contributors, *J. Nucl. Mater.* 463 (2015) 157.
- [13] K. Schmid, K. Krieger, S.W. Lisgo, G. Meisl, S. Brezinsek, JET EFDA Contributors, *J. Nucl. Mater.* 463 (2015) 66–72.
- [14] J. Beal, A. Widdowson, K. Heinola, A. Baron-Wiechec, K.J. Gibson, J.P. Coad, E. Alves, B. Lipschultz, A. Kirschner, H.G. Esser, G.F. Matthews, S. Brezinsek, JET Contributors, *Phys. Scr.* T167 (2016) 014061. <http://dx.doi.org/10.1088/0031-8949/T167/1/014052>.
- [15] A. Kirschner, D. Matveev, D. Borodin, M. Airila, S. Brezinsek, M. Groth, S. Wiesen, A. Widdowson, J. Beal, H.G. Esser, J. Likonen, N. Bekris, R. Ding, JET-EFDA Contributors, *J. Nucl. Mater.* 463 (2015) 116–122.
- [16] C. Ruset, E. Grigore, C. Luculescu, I. Tiseanu, J. Likonen, M. Mayer, M. Rubel, G.F. Matthews, JET Contributors, *Phys. Scr.* T 167 (2016) 014049.
- [17] A. Lasa, K. Heinola, K. Nordland, *Nucl. Fus.* 54 (2014) 083001.
- [18] A. Lasa, K. Heinola, K. Nordland, *Nucl. Fus.* 54 (2014) 123021.
- [19] G.J. van Rooij, J.W. Coenen, L. Aho-Mantila, S. Brezinsek, M. Clever, R. Dux, M. Groth, K. Krieger, S. Marsen, G.F. Matthews, A. Meigs, R. Neu, S. Potzel, T. Pütterich, J. Rapp, M.F. Stamp, the ASDEX Upgrade Team and JET-EFDA Contributors, *J. Nucl. Mater.* 438 (2013) S42–S47.
- [20] H. Maier, M. Rasinski, U von Toussaint, H. Greuner, B. Bösowirth, M. Balden, S. Elgeti, C. Ruset, G. F. Matthews and JET Contributors, *Phys. Scr.* T167 (2016) 014048. <http://dx.doi.org/10.1088/0031-8949/T167/1/014048>.